18th Australasian Fluid Mechanics Conference
Launceston, Australia
3-7 December 2012

Rayleigh-Bénard Roll Formation in a Thermal Intrusion

S. E. Norris[1]

[1]Department of Mechanical Engineering
University of Auckland, Auckland 1142, New Zealand

Abstract

If natural convection in a side heated cavity is initiated by the impulsive heating of one of the side walls, a thermal plume rises up the heated wall and forms a thermal intrusion flowing across the top of the cavity. Experimental data has revealed longitudinal structures in the intrusion. These are thought to be Rayleigh-Bénard convection rolls aligned with the direction of the intrusion flow, formed by the unstable stratification of the intrusion flow.

A three-dimensional CFD simulation of the flow has revealed similar structures to those in the experiment, but with shorter rolls that do not span the full width of the cavity. However, by modelling the lid of the cavity as a conducting solid, the instability of the intrusion is increased and the simulated roll structures occupy the length of the cavity. The roll formation process is therefore shown to be dependent on the thermal boundary condition at the top wall.

Introduction

Natural convection in a side heated cavity is a classical heat transfer problem with a wealth of literature written on the flow problem. The earliest analysis of the problem is that of Batchelor [4] who drew upon the little experimental data available at that time. This was followed by the first numerical computation of the flow field by Poots [11], who used a spectral method and two female assistants as a computational engine. The earliest models to run on an electronic computer were those by Wilkes and Churchill [14] and de Vahl Davis [5], both modelling flow in a two–dimensional square cavity, the former modelling the problem with a transient code, whilst the latter author modelled the flow at steady state. The flow was later modelled by de Vahl Davis and Mallinson in a three-dimensional cavity [7], while the two dimensional steady state problem is a standard benchmark for CFD codes [6].

All these early works concentrated on the problem as a steady state process, with the transient process of imposing a temperature gradient on an initially isothermal and stationary flow being ignored or used as a numerical device to achieve the steady state solution. This was rectified by a numerical and scaling study of the transient flow by Patterson and Imberger [10], followed by a series of numerical and experimental studies of the two-dimensional transient flow by Patterson with Armfield and Schöpf [9, 3, 12]. Whilst these studies provided an understanding of the structure of the fundamental two-dimensional flow in the cavity, an experiment by Schöpf and Stiller [13] revealed an interesting three-dimensional structure of the initial thermal intrusion. Shadowgraphs taken looking down on the intrusion flow showed longitudinal structures in the intrusion, which were thought to be rolls formed by a Rayleigh-Bénard instability.

Problem Description

An initially isothermal and motionless fluid is confined to a cavity of square cross section. The left wall is impulsively heated creating a thermal boundary layer that rises up the heated wall and intrudes into the cavity along the roof of the cavity. A schematic of the experiment is shown in figure 1.

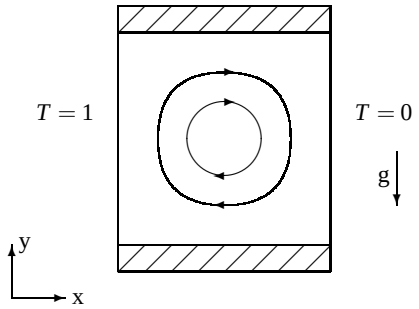

Figure 1: Natural Convection in a square side heated cavity.

For the classical side-heated cavity problem, with adiabatic upper and lower boundaries, the flow is characterised by two dimensionless groups; the Rayleigh number,

$$\mathrm{Ra} = \frac{g\beta\Delta T\, l^3}{\nu\alpha}, \tag{1}$$

and the Prandtl number,

$$\mathrm{Pr} = \frac{\nu}{\alpha}, \tag{2}$$

where g is the acceleration due to gravity, β the thermal expansion coefficient, ΔT the temperature difference across the cavity, l the length scale of the cavity (the width or height of the cavity), and ν and α the kinematic viscosity and the thermal diffusivity respectively.

The time scale has been non-dimensionalised with respect to the viscosity and the cavity length scale using a viscosity based Fourier number scaling

$$\tau = \frac{\nu t}{l^2}, \tag{3}$$

while the velocity has been similarly treated,

$$U = \frac{u l}{\nu}, \tag{4}$$

with U being the Fourier velocity.

The effect of the conducting upper boundary of the cavity is explored in this study. This can be characterised by the ratio of the timescales of conduction across the wall and convection of the intrusion parallel to the wall.

$$N_w = \frac{\nu w^2}{\alpha_w l^2} \tag{5}$$

Here w and α_w are the thickness and thermal diffucivity of the conducting boundary, and ν and l are as above. As $N_w \to 0$

the effect of conduction in the wall becomes negligable, and the boundary behaves as an adiabatic boundary.

The experiments of Patterson and that of Schöpf and Stiller all used a cavity with a width and height of 0.24m, and a length in the z axis of 0.5m. The hot and cold side walls were constructed of 1mm copper plates, whilst the remaining boundaries were constructed with 19mm Perspex sheets, allowing the visualisation of the flow within the cavity. Water was used as the working fluid. The numerical results will be compared to the Schöpf experiments for which the ambient temperature of the surroundings and the initial temperature of the cavity and fluid was approximately 21°C. The left wall of the cavity was impulsively heated by a temperature increase in the range of 1 to 7°C, whilst the right wall was maintained at the ambient temperature. For the case of a temperature increase of $\Delta T = 4.8$°C this results in a Rayleigh number for the cavity of $\mathrm{Ra} = 10^9$, and a Prandtl number of $\mathrm{Pr} = 6.8$, and $N_w = 0.04$.

Numerical Model

The flow was modelled using the in-house SnS code [1, 8], a Cartesian non-staggered mesh, finite volume solver. The momentum and temperature equations were discretised using the QUICK third order upwind differencing scheme, and an Adams-Bashforth based fractional step scheme [2] was used to advance the solution in time. The time step was limited to ensure that the maximum Courant number at no time exceeded 0.1.

The initial flow field was set to be motionless and isothermal, with $u = v = w = T = 0$. The left and right boundaries were modelled as isothermal walls with a no-slip boundary condition for velocity. At time $t = 0$ the left x boundary was set to $T = 1$, while the opposite boundary remained at $T = 0$, the same temperature as the cavity interior. Two types of boundary condition were imposed at the upper and lower surfaces. Initial runs were made with the boundaries being modelled as adiabatic no-slip walls. However, in order to more correctly model the experimental cavity, the upper and lower boundaries were modified to be conducting solid walls with a thickness equal to $19/240$ of the cavity width, with an adiabatic boundary condition on the outer surface of the wall.

Both two- and three dimensional models of the flow were modelled. For the three dimensional problem periodic boundary conditions were used in the z axis to ensure any disturbances in this axis were due to instabilities in the flow and not due to end wall effects.

To trigger three dimensional structures in the flow a random fluctuation in the range of $\Delta T = \pm 0.1$ was added to the left wall for the initial time step only.

Results and Discussion

Isotherms and streamlines for a two-dimensional flow are shown in figure 3 for a fluid impulsively heated at the left boundary, plots being given at $\tau = 0.51 \times 10^{-3}$, 0.86×10^{-3} and 1.2×10^{-3}. At $\tau = 0.51 \times 10^{-3}$ a thermal boundary layer has formed on the left side of the cavity, which has generated an intrusion that is starting to cross the cavity below the upper boundary. For the middle plots, at $\tau = 0.86 \times 10^{-3}$, the intrusion has crossed two-thirds of the cavity, whilst for the final plots, at $\tau = 1.2 \times 10^{-3}$, the intrusion has reached the far wall and a body of heated fluid lies below the upper boundary across the full width of the cavity.

Simulated shadowgraphs of the flow looking down on the intrusion are shown in figure 2. These were visualised at $\tau = 0.51 \times 10^{-3}$ and $\tau = 1.33 \times 10^{-3}$. They should be compared with the shadowgraphs taken at 30s and 78s in Schöpf and Stiller [13]. In the first simulated shadowgraph the thermal intrusion has only just started to move across the upper boundary of the cavity. The leading edge of this thermal intrusion can be seen as a vertical white line in the left side of the image. The second simulated shadowgraph image shows the flow as the thermal intrusion reaches the far side of the cavity. A pattern of light and dark regions aligned with the flow direction have appeared in the intrusion.

A close examination of the isotherms for the modelled flow in figure 3 at $\tau = 1.2 \times 10^{-3}$ reveals that an unstable thermal gradient exists between the core of the thermal intrusion and the top of the cavity. It is thought that the structures seen in the shadowgraph arise from Rayleigh–Bénard cells forming with their axes aligned in the flow direction.

For Rayleigh–Bénard convection between a rigid and a free boundary, which corresponds to the boundary conditions for a convection roll in the upper layer of the intrusion, the critical Rayleigh number is $\mathrm{Ra}_c = 1100$. If the structures seen in the experimental images are a result of a Rayleigh–Bénard instability, the intrusion Rayleigh number, based on the temperature difference and the vertical extent of the region over which the intrusion is unstable, must be greater than this critical Rayleigh number.

Initial calculations for the flow were made using an adiabatic upper boundary, corresponding to $N_w = 0$. However, the intrusion Rayleigh number for these simulations gave a number much lower than the critical value. It was decided to recalculate the problem using a more realistic boundary condition for the upper and lower boundaries, with the upper and lower surfaces being modelled as conducting slabs of Perspex, having a thickness of $19/240$ of the cavity width, giving $N_w = 0.04$. The slabs had an adiabatic boundary condition on their outer surfaces.

The two-dimensional flow shown in figure 3 is in fact calculated with the modified boundary condition, and at this scale it is all but indistinguishable from the flow with the adiabatic boundaries. The differences between the two solutions is seen in figure 4, where the vertical scale has been expanded to reveal the increased vertical temperature gradient in the simulation with a conducting boundary. From inspection the temperature gradient for the conducting boundary flow is much higher midway along the intrusion, although both are similar at the intrusion head. This is borne out in figure 5 which shows the intrusion Rayleigh number. This is similar for both boundary conditions at the head of the intrusion. However, in the remainder of the intrusion the conducting boundary case has a higher intrusion

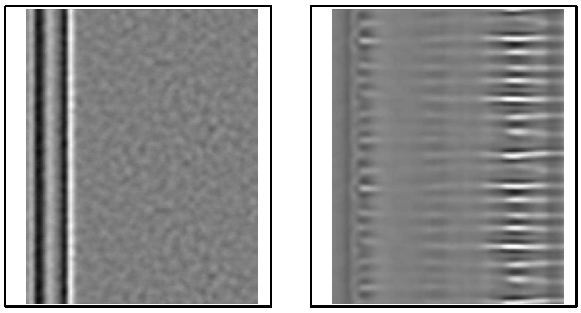

Figure 2: Simulated shadowgraphs of a thermal intrusion moving across a cavity. Looking down on the cavity at $\tau = 0.51 \times 10^{-3}$ (left) and $\tau = 1.33 \times 10^{-3}$ (right), for a flow with $\mathrm{Ra} = 10^9$.

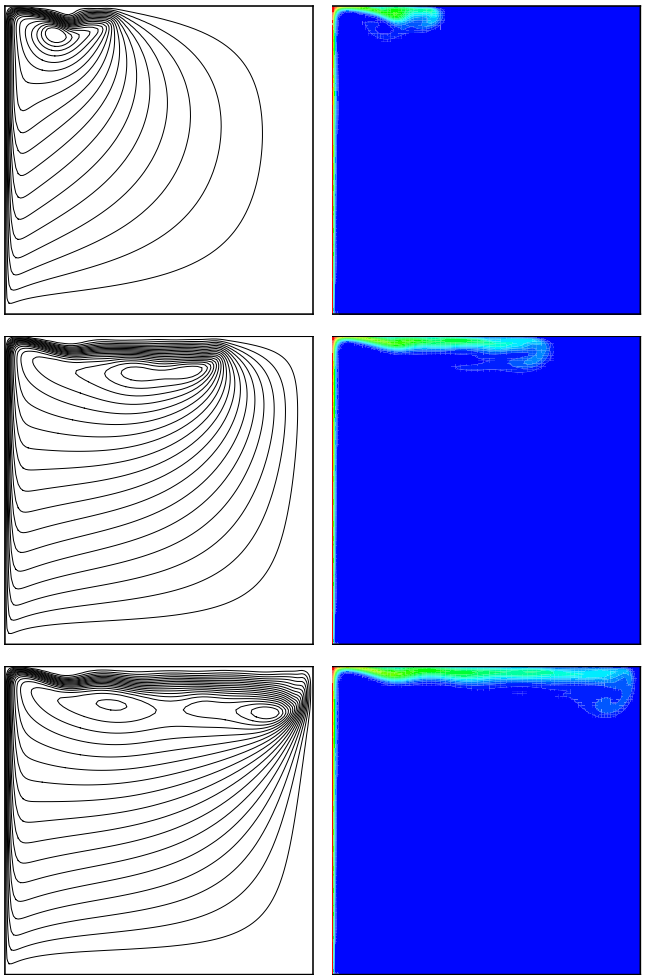

Figure 3: Numerical two-dimensional model of the intrusion flow, with streamlines on the left, isotherms on the right, for a flow with $\mathrm{Ra} = 10^9$, $\mathrm{Pr} = 6.7$ at $\tau = 0.51 \times 10^{-3}$, 0.86×10^{-3} and 1.2×10^{-3}.

Rayleigh number than the adiabatic boundary case, with the intrusion Rayleigh number exceeding the critical Rayleigh number $\mathrm{Ra}_c = 1100$ for most of the extent of the intrusion. In contrast, in the simulation made with an adiabatic upper boundary the intrusion Rayleigh number exceeds the critical Rayleigh number only in the head region.

The three dimensional structure of the intrusion flow is illustrated in figure 8, with isolines of w plotted at the $x = 0.214, 0.352, 0.616, 0.821$ and 0.920 sections, along with plots of the u velocity profile and temperature gradient at each section. The double row of velocity contours shown along the upper boundary has a similar structure to that of a two dimensional Rayleigh–Bénard flow. The rolls are a secondary feature of the flow, with the w velocity in the intrusion having a much lower value than u. For the $\mathrm{Ra} = 10^9$, $\mathrm{Pr} = 6.7$ flow shown in figure 8 w is in the range ± 0.015 whilst the u velocity reaches a maximum of 6.6.

The depth of the intrusion at the instant it reaches the far wall of the cavity is shown in figure 6, for cavity Rayleigh numbers in the range $\mathrm{Ra} = 5 \times 10^7$ to $\mathrm{Ra} = 1.2 \times 10^9$. The intrusion depth is seen to decrease with increasing Rayleigh number.

The experiments of Schöpf and Stiller [13] revealed that the wavelengths of the rolls in the thermal intrusion decreased with an increasing cavity Rayleigh number. If the aspect ratio of the

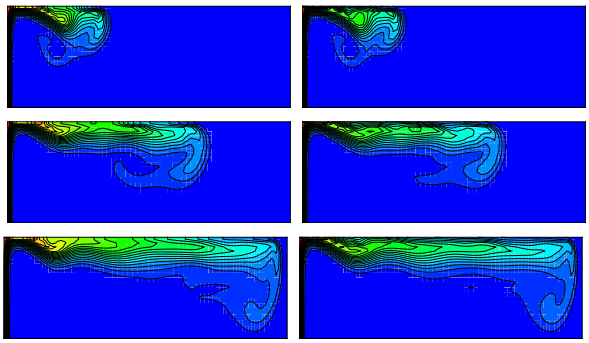

Figure 4: Numerical two-dimensional model of the intrusion flow. Isotherms for a flow with $\mathrm{Ra} = 10^9$, $\mathrm{Pr} = 6.7$ at $\tau = 0.51 \times 10^{-3}$, 0.86×10^{-3} and 1.2×10^{-3}, are shown with an expanded vertical scale, with only the top 0.18 of the cavity being shown. $N_w = 0$ left, $N_w = 0.04$ right.

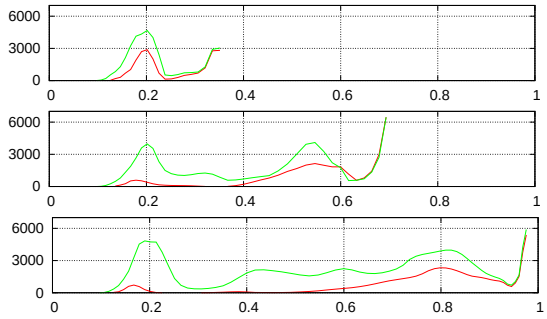

Figure 5: The intrusion Rayleigh number, based on the temperature difference and thickness of the intrusion. The critical Rayleigh number is approximately $\mathrm{Ra}_c = 1100$. Plots are given for $N - w = 0$ (red) and $N_w = 0.04$ (green), at $\tau = 0.51 \times 10^{-3}$, 0.86×10^{-3} and 1.2×10^{-3}.

rolls remain constant, then the decreasing thickness of the intrusion at higher Rayleigh number will result in this decreased wavelength. To model this trend, runs were made with the conducting upper boundaries for Rayleigh numbers in the range of $\mathrm{Ra} = 5 \times 10^7$ to $\mathrm{Ra} = 1.2 \times 10^9$. The wavelengths of the rolls in the modelled flow are shown in figure 7. While both the numerical and experimental wavelengths decrease with increasing Rayleigh number, they differ in magnitude by up to 50%.

Conclusions

A transient intrusion flow in a three-dimensional side heated cavity has been modelled using a fractional-step finite volume code. The CFD code was used to recreate the experiments of Schöpf and Stiller[13] and it successfully captured the Rayleigh–Bénard rolls that form in the intrusion. The wavelength of the calculated rolls were in error when compared to the experiment, but displayed the same trend of decreasing wavelength with increasing Rayleigh number. The generation of the rolls was shown to depend on the upper boundary not being truly adiabatic in the experiment, with the thermal capacity of the boundary increasing the temperature gradient across the intrusion initiating stronger and more extensive rolls.

References

[1] Armfield, S., Norris, S., Morgan, P. and Street, R., A parallel non-staggered Navier-Stokes solver implemented on a workstation cluster, in *CFD 2002*, editors S. Armfield, P. Morgan and K. Srinivas, Springer–Verlag, 2003, 30–45.

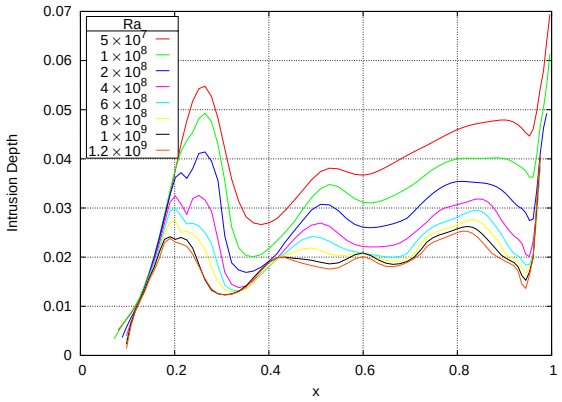

Figure 6: The intrusion depth as the intrusion reaches the right wall of the cavity, for flows with cavity Rayleigh numbers in the range of $\mathrm{Ra} = 5\times10^7$ to 1.2×10^9. Calculated with conducting boundaries, $N_w = 0.04$.

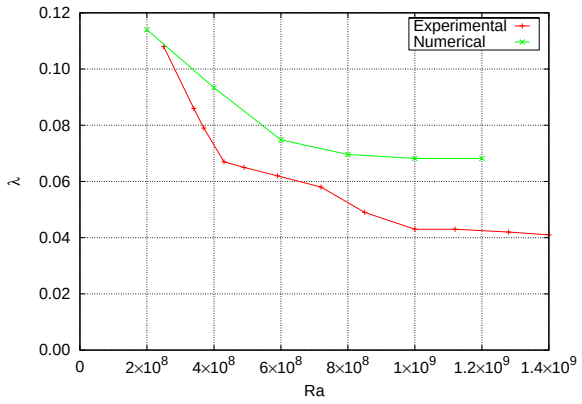

Figure 7: Wavelength of the intrusion rolls for the numerical model and the experiment of Schöpf and Stiller[13].

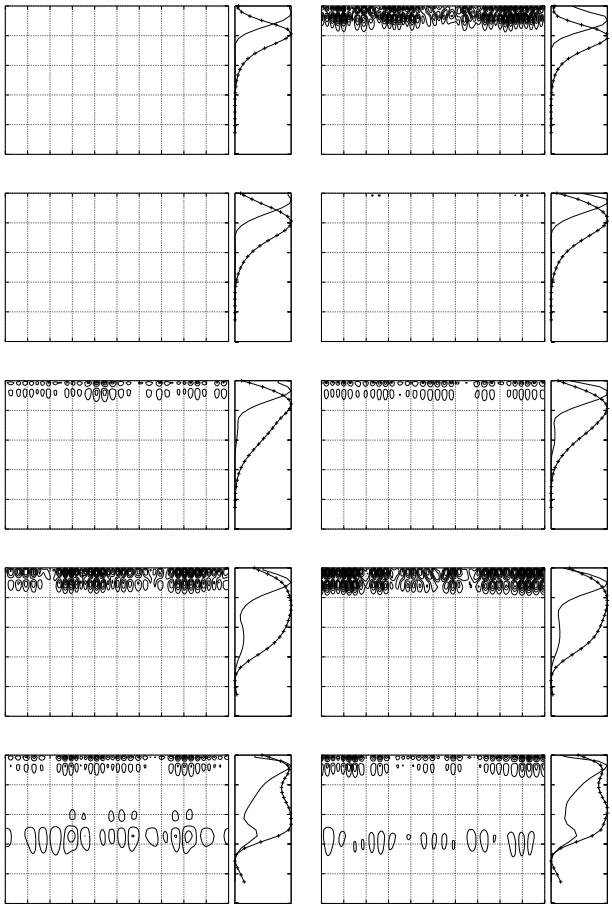

Figure 8: Sections normal to the x axis taken through the cavity for $N_w = 0$ (left) and $N_w = 0.04$ (right). Sections are taken at $x = 0.214, 0.352, 0.616, 0.821$ and 0.920, with only the top 0.25 of the cavity being shown. For each graph the contours of w velocity are shown, with the contours being at 0.0010 intervals in the range ±0.0105, along with profiles of the u velocity (the crossed line) and the temperature (the solid line). Profiles are for flows with $\mathrm{Ra} = 10^9$ and $\mathrm{Pr} = 6.7$ at $\tau = 1.2\times10^{-3}$.

[2] Armfield, S. and Street, R., An analysis and comparison of the time accuracy of fractional-step methods for the Navier-Stokes equations on staggered grids, *International Journal for Numerical Methods in Fluids*, **38**, 2002, 255–282.

[3] Armfield, S. W. and Patterson, J. C., Wave properties of natural-convection boundary layers, *Journal of Fluid Mechanics*, **239**, 1992, 195–211.

[4] Batchelor, G. K., Heat transfer by free convection across a closed cavity between vertical boundaries at different temperatures, *Quarterly Journal of Applied Mathematics*, **12**, 1954, 209–233.

[5] de Vahl Davis, G., Laminar natural convection in an enclosed rectangular cavity, *International Journal of Heat and Mass Transfer*, **11**, 1968, 1674–1693.

[6] de Vahl Davis, G., Natural convection of air in a square cavity: A bench mark numerical solution, *International Journal for Numerical Methods in Fluids*, **3**, 1983, 249–264.

[7] Mallinson, G. D. and de Vahl Davis, G., Three-dimensional natural convection in a box: A numerical study, *Journal of Fluid Mechanics*, **83**, 1977, 1–31.

[8] Norris, S. E., *A Parallel Navier–Stokes Solver for Natural Convection and Free Surface Flow*, PhD thesis, University of Sydney, 2000.

[9] Patterson, J. C. and Armfield, S. W., Transient features of natural convection in a cavity, *Journal of Fluid Mechanics*, **219**, 1990, 469–497.

[10] Patterson, J. C. and Imberger, J., Unsteady natural convection in a rectangular cavity, *Journal of Fluid Mechanics*, **100**, 1980, 65–86.

[11] Poots, G., Heat transfer by laminar free convection in enclosed plane gas layers, *Quarterly Journal of Mechanics and Applied Mathematics*, **11**, 1958, 257–273.

[12] Schöpf, W. and Patterson, J. C., Natural convection in a side-heated cavity: visualization of the initial flow features, *Journal of Fluid Mechanics*, **295**, 1995, 357–379.

[13] Schöpf, W. and Stiller, O., Three-dimensional patterns in a transient, stratified intrusion flow, *Physical Review Letters*, **79**, 1997, 4373–4376.

[14] Wilkes, J. O. and Churchill, S. W., The finite-difference computation of natural convection in a rectangular enclosure, *American Institute of Chemical Engineers Journal*, **12**, 1966, 161–166.